International Journal of Trend in Research and Development, Volume 13(3), ISSN: 2394-9333
www.ijtrd.com

Catalytic Degradation of Tetracycline Hydrochloride Using Novel Rod-Like Nanosheet MoS_2

Chong Li
School of Materials Science and Engineering, Henan Polytechnic University, Henan, Jiaozuo, China

Abstract: In this study, nanoflake-structured MoS_2 (MoS_2 NSs) was successfully prepared via a one-step hydrothermal method. The as-synthesized MoS_2 NSs shows a hollow rod-like morphology with enlarged interlayer spacing and abundant lattice dislocations, which can effectively improve the number of active sites and electron transport efficiency through dislocation synergistic effect. MoS_2 NSs exhibits excellent catalytic performance for peroxymonosulfate (PMS) activation to degrade tetracycline hydrochloride (TCH). Under optimal conditions (pH=3), the degradation efficiency of TCH reaches over 95% within 60 min. The system remains efficient and stable under a wide pH range and in the presence of common inorganic anions. Radical quenching experiments verify that TCH degradation is dominated by multiple reactive oxygen species including ·OH, SO_4 •⁻ , O_2 •⁻ , and $^1O_2$. MoS_2 NSs possesses good reusability and stability, providing a feasible strategy for efficient treatment of antibiotic wastewater.

Keywords*: MoS_2 ; Fenton-like; peroxymonosulfate; tetracycline hydrochloride*

I. INTRODUCTION

As a broad-spectrum antibiotic, tetracycline hydrochloride (TCH) is widely used in medicine and veterinary medicine due to its low cost and good antibacterial effect. However, TCH has high water solubility, which easily causes serious pollution to aquatic and soil ecosystems, threatening human health [1-2]. Therefore, it is urgent to develop efficient and safe degradation technologies to address the environmental impact of antibiotics. Advanced oxidation processes (AOPs) are efficient and eco-friendly wastewater treatment technologies that can mineralize macromolecular organic pollutants into water and CO_2 by generating hydroxyl radicals, with the advantages of easy operation, low cost, and no secondary pollution. Among various AOPs, activated persulfate (PS) oxidation is currently the most popular method, because sulfate radicals (SO_4 •⁻) produced by the cleavage of peroxide bonds in PS exhibit better stability, longer half-life, and higher oxidation potential than hydroxyl radicals (•OH)[3[5]. Thus, activated PS technology has become an effective method for antibiotic degradation. Notably, persulfate (PS) includes peroxymonosulfate (PMS) and peroxydisulfate (PDS).

Molybdenum disulfide (MoS_2) is a layered material with excellent physicochemical properties, showing outstanding performance in hydrogen evolution and catalysis. Nevertheless, the inert basal plane of MoS_2 results in active sites only existing at the edge sites, leading to low electron transfer efficiency and limiting its application in antibiotic removal[6-7].Enlarging the interlayer spacing of MoS_2 is a common strategy to enhance catalytic activity. Cai et al.[8] prepared CTAB-assisted MoS_2 -based composites with expanded interlayer spacing, which exhibited good adsorption performance for Cr^{6+} and Ni^{2+} . Zhao et al. [9]coated MoS_2 nanosheets on porous γ-Al_2O_3 , providing abundant adsorption sites for Hg^0 capture. In addition, biochar was used to support MoS_2 nanosheets to avoid agglomeration, and the obtained MoS_2 -modified magnetic biochar showed favorable adsorption capacity for Cd in aqueous solution. Li et al.[10] synthesized hollow Co_3S_4 -MoS_2 composite adsorbents via hydrothermal method. The excellent TCH adsorption performance of Co_3S_4 -MoS_2 was mainly attributed to multiple interactions induced by abundant functional groups, including surface complexation, π-π interaction, and hydrophobicinteraction. Although the reported MoS_2 -based composites have increased functional groups and active sites, thus improving adsorption and catalytic performance, their complex preparation and high cost restrict large-scale application.

In this work, nanoflake-structured MoS_2 (MoS_2 NSs) was prepared via a one-step hydrothermal method, and its performance in activating PMS for TCH removal was investigated. Compared with flower-like MoS_2 (MoS_2 NFs), MoS_2 NSs possesses wider interlayer spacing and higher-density interlayer dislocations. The larger interlayer spacing exposes more catalytic active sites, while interlayer dislocations connect adjacent layers to ensure efficient charge transport inside and outside the catalyst. Therefore, the synergistic effect enables MoS_2 NSs to efficiently activate PMS for antibiotic degradation.

II. EXPERIMENTAL SECTION

A. Synthesis of the MoS_2 nanotubes composed of MoS_2 NSs

1.2 mmol of sulfur powder and 0.075 mmol of ammonium molybdate [$(NH_4)_6Mo_7O_{24}$] were dissolved in a mixture of 13 mL anhydrous ethanol and 14 mL octylamine. After being thoroughly stirred, the mixture was transferred into a Teflon-lined autoclave. The autoclave was then heated at 200 ℃ for 24 h in a blast drying oven. After the reaction, the oven was turned off and the autoclave was cooled to room temperature naturally. The product was collected by centrifugation, washed with anhydrous ethanol several times, and dried under vacuum for 12 h to obtain the final sample.

B. Characterizations

The surface morphology of the catalyst was characterized by scanning electron microscopy (SEM, QUANTA 250, FEI, Czech Republic) and transmission electron microscopy (TEM, JEM 2100, JEOL, Japan). The crystal structure of the sample was analyzed by X-ray diffractometer (XRD, D8 ADVANCE, Bruker, Germany).

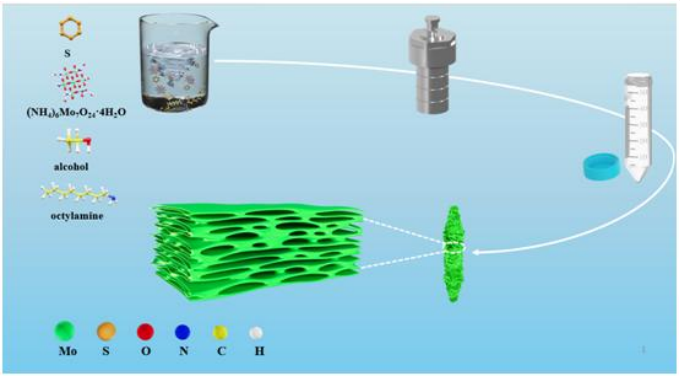

Scheme 1. Schematic illustration of the fabrication processes of MoS_2 nanotubes composed of MoS_2 NSs.

III. RESULTS AND DISCUSSION

A..Preparation and structural characterization

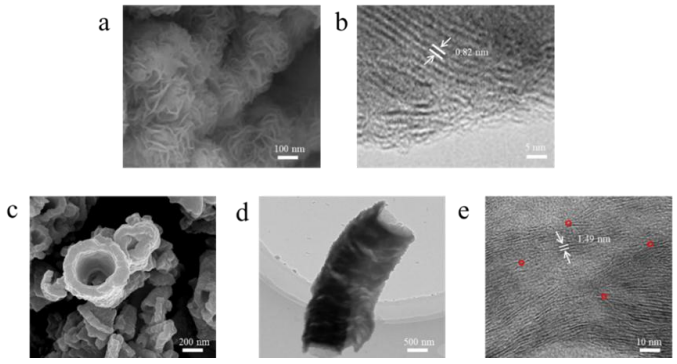

Fig.1. (a) SEM image of MoS_2 NFs. (b) HRTEM image of MoS_2 NFs. (c) SEM image of MoS_2 NSs. (d)TEM image of MoS_2 NSs. (e)HRTEM image of MoS_2 NSs.

Fig. 1(a) and (b) show the SEM and HRTEM images of MoS_2 NFs. As clearly observed in Fig.1(a), the as-prepared MoS_2 NFs display a typical flower-like morphology. The wrinkled structure of the petals enlarges the exposed edge area of the material and provides abundant active sites for the catalyst. Fig. 1(b) presents the HRTEM image of MoS_2 NFs, in which distinct lattice fringes can be seen with a lattice spacing of 0.82 nm.Fig. 1(c) displays the SEM image of MoS_2 NSs. It can be observed that MoS_2 NSs are hollow rod-like structures formed by the continuous stacking of numerous nanosheets. The hollow morphology allows full contact between the catalyst, oxidants and pollutants, and both the interior and exterior surfaces can provide active sites for the degradation process. Fig.1(d) further confirms the rod-like morphology of MoS_2 NSs.Fig. 1(f) shows the HRTEM image of MoS_2 NSs, with a lattice spacing of 1.49 nm, which is larger than the 0.82 nm of MoS_2 NFs. The increased lattice spacing not only provides more active sites for catalytic degradation but also improves the adsorption performance of the sample. In addition, a large number of Y-shaped structures and lattice defects (marked by red circles) exist in Fig. 1(f). These Y-shaped structures enhance the interlayer electron transport and supply sufficient electrons for the catalyst and oxidants.

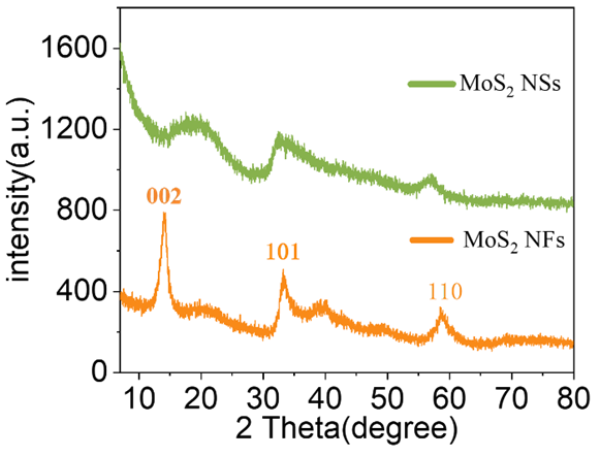

Fig. 2. XRD patterns of MoS_2 NFs and MoS_2 NSs

The crystal structures of MoS_2 NFs and MoS_2 NSs were further investigated by X-ray diffraction (XRD). As can be seen in Fig. 2, the diffraction peaks at 2θ = 19.09°, 34.51°, and 57.42° correspond to the (002), (101), and (110) crystal planes of MoS_2 NFs, respectively, confirming the successful preparation of MoS_2 NFs.In addition, the characteristic peaks of MoS_2 NSs are basically consistent with those of MoS_2 NFs. However, the diffraction peaks of MoS_2 NSs show decreased intensity, widened width, and slight shift. This is attributed to the stacking of nanosheets during synthesis, which causes lattice distortion and generates abundant defects in MoS_2 NSs[11-12].

B. TCH Degradation: Results and Discussion

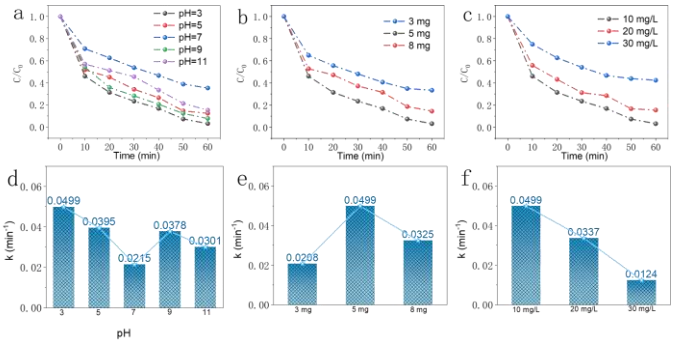

Fig.3. (a)Effect of different pH values on degradation performance. (b)Effect of catalyst dosage on degradation performance. (c)Effect of different TCH concentrations on degradation performance. (d-f)Histograms of kinetic constants for various influencing factors.

It has been reported that the traditional Fenton reaction is limited by •OH radicals, resulting in restricted large-scale application under acidic and alkaline conditions. Therefore, to investigate the TCH degradation performance of the MoS_2 NSs/PMS system at different pH values, experiments were carried out at pH = 3, 5, 7, 9, and 11. As shown in Fig. 3(a), the TCH degradation efficiency reaches 62.4% at pH = 7 , with a corresponding kinetic constant k of 0.0215 min^{-1}. The unsatisfactory efficiency is attributed to the deprotonated HSO_5^- from PMS under neutral conditions, which has uniform electron distribution and requires higher energy for O–O bond cleavage, leading to a sharp decrease in active species. In acidic medium, the degradation efficiency reaches 97.3% with k = 0.0499 min^{-1}, because protonated HSO_5^- shows enhanced polarity of the O–O bond and is readily

activated. The degradation efficiency is 92.7% at pH = 9 and decreases to 83.3% at pH = 11, accompanied by a decline of k from 0.0378 to 0.0301 min^{-1}. A high concentration of OH^- promotes O–O bond cleavage of PMS to produce ·OH, and SO_4 ·$^-$ also reacts with OH^- to generate ·OH. However, excessive OH^- at pH = 11 causes quenching of ·OH and massive consumption of SO_4 ·$^-$. These results confirm the broad pH applicability of the system, with the optimal performance at pH = 3.

To explore the effect of catalyst dosage on TCH degradation, Fig. 3(b) presents degradation curves at pH = 3 and TCH concentration of 10 mg/L with three catalyst dosages. The degradation efficiency is 61.5% (k = 0.0208 min^{-1}) at 3 mg catalyst, increases to 97.3% at 5 mg, and decreases with further addition. Excessive catalyst causes mutual shielding and reduces the exposure of active sites. The influence of TCH concentration was also studied. With TCH concentrations of 10, 20, and 30 mg/L, the degradation efficiency decreases from 97.3% to 43.8%, because the amount of active species generated from PMS is fixed under identical conditions, and excessive TCH cannot be fully degraded due to insufficient active species.

Numerous anions commonly exist in natural water. To evaluate the practical performance, anti-interference experiments were conducted using four typical inorganic anions (NaCl, NaBr, $NaHCO_3$, and NaH_2PO_4). As shown in Fig. 4(a), NaCl, $NaHCO_3$, and NaH_2PO_4 have little influence on TCH degradation, indicating excellent anti-interference ability of the MoS_2 NSs/PMS system. However, the addition of NaBr reduces the degradation efficiency to 63.4% with k = 0.0152 min^{-1}, which is mainly due to the reaction between Br^- and ·OH to form weakly oxidative Br·.

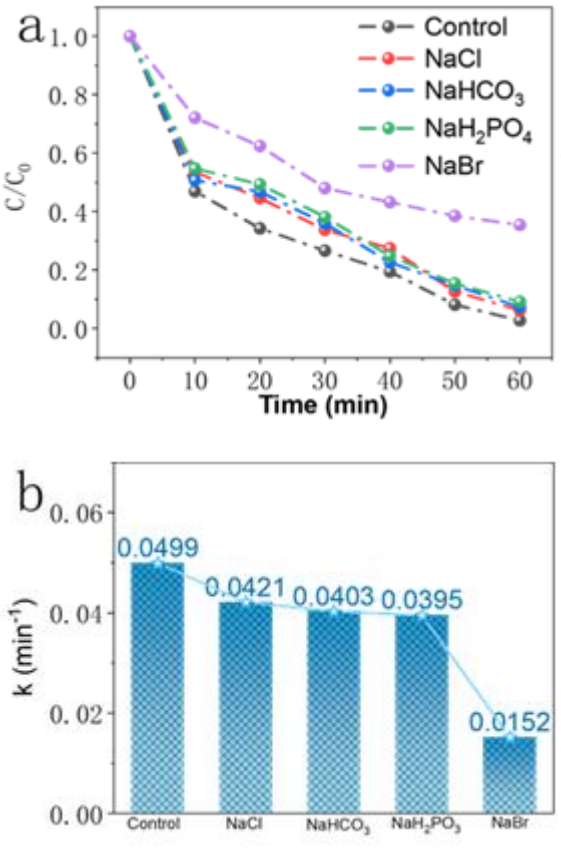

Fig.4. (a)Effect of different anions on TCH degradation. (b)Histogram of reaction kinetic constants.

To identify the dominant reactive species responsible for TCH removal in the MoS_2 NSs/PMS system, radical quenching experiments were carried out using various scavengers. Specifically, isopropanol (IPA) was used as the scavenger for ·OH, methanol (MeOH) for SO_4 •$^-$ and ·OH, p-benzoquinone (PBQ) for O_2 •$^-$, and furfuryl alcohol (FFA) for $^1O_2$. As shown in Fig. 5(a), the TCH degradation efficiency decreased significantly after adding these scavengers. With the addition of IPA, MeOH, PBQ, and FFA, the TCH degradation efficiencies were 56.4% (k = 0.0132 min^{-1}), 38.2% (k = 0.0098 min^{-1}), 26.8% (k = 0.0076 min^{-1}), and 23.1% (k = 0.0051 min^{-1}), respectively. These results confirm that ·OH, SO_4 •$^-$, O_2 •$^-$, and $^1O_2$ are all involved in TCH degradation, among which O_2 •$^-$ and $^1O_2$ play the primary roles, which is consistent with our previous radical probe experiments[13].

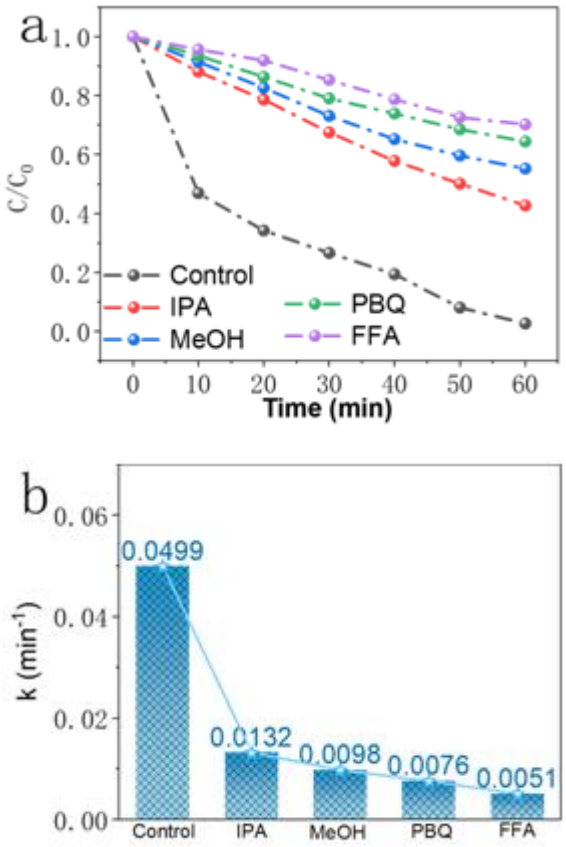

Fig. 5. (a)Effect of sacrificial agents on TCH degradation. (b)Histogram of reaction kinetic constants.

C. Mechanism analysis

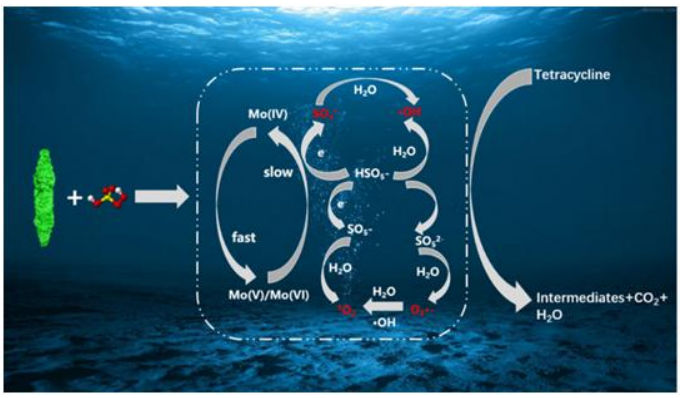

Scheme 2.Schematic mechanism of TCH degradation over MoS_2 nanotubes constructed from MoS_2 NSs

Based on the above experimental results and discussion, the reaction mechanism of TCH degradation in the MoS_2

NSs/PMS system can be briefly proposed. Firstly, abundant H^+ in water reacts with unsaturated S atoms on the catalyst surface to generate H_2S, leading to the exposure of surface Mo^{4+}. Electron transfer occurs between Mo^{4+} and adsorbed PMS, promoting the decomposition of PMS into HSO_5^- and Mo^{5+}/Mo^{6+}. Meanwhile, HSO_5^- further reacts to produce radical and non-radical species. Specifically, $O_2^{\bullet-}$ reacts with H_2O and ·OH to generate non-radical $^1O_2$, and part of ·OH is derived from the reaction between $SO_4^{\bullet-}$ and H_2O[14-15].

CONCLUSIONS

In this study, a novel nanoflake-structured MoS_2 material (MoS_2 NSs) was successfully synthesized via a facile one-pot hydrothermal method using ammonium molybdate, sulfur powder, ethanol, and octylamine as raw materials. Compared with flower-like MoS_2 (MoS_2 NFs), the as-prepared MoS_2 NSs exhibits a unique rod-like hollow morphology assembled by nanosheets, with expanded interlayer spacing and abundant interlayer dislocations. Such structural features endow MoS_2 NSs with more exposed active sites and accelerated charge transfer, thereby significantly boosting the activation of peroxymonosulfate (PMS).

The catalytic degradation experiments demonstrate that the MoS_2 NSs/PMS system exhibits excellent performance for tetracycline hydrochloride (TCH) removal. Under the optimal condition of pH=3, the degradation efficiency of TCH reaches 80% within 30 min and exceeds 95% at 60 min. The system maintains favorable catalytic activity over a wide pH range and shows strong anti-interference ability against common inorganic anions. Radical quenching tests confirm that TCH degradation is dominated by a multi-reactive oxygen species pathway involving $SO_4^{\cdot-}$, $^1O_2$, $O_2^{\cdot-}$, and ·OH. Moreover, MoS_2 NSs presents satisfactory reusability and structural stability during cycling tests.

This work provides a simple and effective strategy for constructing high-performance MoS_2 -based catalysts for PMS activation, which offers a promising reference for the efficient degradation of antibiotic pollutants in wastewater treatment.

References

[1] He C, Zhou J, Yang C, et al. Accumulation, transportation, and distribution of tetracycline and cadmium in rice[J]. Journal of Environmental Sciences, 2023, 126: 58-69.

[2] Wang K, Yang S, Yu X, et al. Effect of microplastics on the degradation of tetracycline in a soil microbial electric field[J]. Journal of Hazardous materials, 2023, 460: 132313.

[3] Chen X, Liu L. PMS activation over MoS2/Co0.75Mo3S3.75 for RhB pollutant oxidation removal in fuel cell system[J]. Journal of Environmental Chemical Engineering, 2022, 10(3): 107449.

[4] Li J, Zhu W, Gao Y, et al. The catalyst derived from the sulfurized Co-doped metal–organic framework (MOF) for peroxymonosulfate (PMS) activation and its application to pollutant removal[J]. Separation and Purification Technology, 2022, 285: 120362.

[5] Yu X, Wu X, Guo F, et al. Visible-light-assisted activation of peroxymonosulfate (PMS) over CoOx @C/g-C3N4 composite for efficient organic pollutant degradation[J]. Journal of Alloys and Compounds, 2023, 948: 169702.

[6] Mohammadi M, Bahadorestani M. Can MoS2 membrane be used for removal of mineral pollutants from water? First-principle study[J]. Materials Science and Engineering: B, 2022, 278: 115642.

[7] Yan Q, Lian C, Huang K, et al. Constructing an acidic microenvironment by MoS2 in heterogeneous Fenton reaction for pollutant control[J]. Angewandte Chemie International Edition, 2021, 60(31): 17155-17163.

[8] Cai W, Dionysiou D D, Fu F, et al. CTAB–intercalated molybdenum disulfide nanosheets for enhanced simultaneous removal of Cr(VI) and Ni(II) from aqueous solutions[J]. Journal of Hazardous materials, 2020, 396: 122728.

[9] Zhao H, Yang G, Gao X, et al. Hg0 capture over CoMoS/γ-Al2O3 with MoS2 nanosheets at low temperatures[J]. Environmental Science & Technology, 2016, 50(2): 1056-1064.

[10] Li S, Chen X, Li M, et al. Hollow Co3S4 polyhedron decorated with interlayer-expanded MoS2 nanosheets for efficient tetracycline removal from aqueous solution[J]. Chemical Engineering Journal, 2022, 441: 136006.

[11] Z. Liu, K. Nie, X. Qu, X. Li, B. Li, Y. Yuan, S. Chong, P. Liu, Y. Li, Z. Yin, W. Huang, General bottom-up colloidal synthesis of nano-monolayer transition-metal dichalcogenides with high 1T ′-phase purity, J. Am. Chem. Soc. 144 (11) (2022) 4863–4873.

[12] H. Wang, X. Xiao, S. Liu, C.L. Chiang, X. Kuai, C.K. Peng, Y.C. Lin, X. Meng, J. Zhao, J. Choi, Y.G. Lin, J.M. Lee, L. Gao, Structural and electronic optimization of MoS 2 edges for hydrogen evolution, J. Am. Chem. Soc. 141 (46) (2019) 18578–18584.

[13] X. Chen, Z. Wang, Y. Wei, X. Zhang, Q. Zhang, L. Gu, L. Zhang, N. Yang, R. Yu, High phase-purity 1T-MoS 2 ultrathin nanosheets by a spatially confined template, Angew. Chem. Int. Ed. Engl. 58 (49) (2019) 17621–17624.

[14] L. Long, H. Zhang, M. Ye, Z. Fang, Ammonia cation-assisted bubble template for synthesizing hollow TiO 2 nanospheres and their application in lithiumion storage, RSC Adv. 5 (16) (2015) 12224–12229.

[15] H. Li, K. Xu, P. Chen, Y. Yuan, Y. Qiu, L. Wang, L. Zhu, X. Wang, G. Cai, L. Zheng, C. Dai, D. Zhou, N. Zhang, J. Zhu, J. Xie, F. Liao, H. Peng, Y. Peng, J. Ju, Z. Lin, J. Sun. Achieving ultrahigh electrochemical performance by surface design and nanoconfined water manipulation. Natl. Sci. Rev. 9(6) (2022) nwac079. https://doi.org/10.1093/nsr/nwac079.